Supplementary Information

Formation and characterization of Synthetic Nanopores

A single nanopore is created in a Si_3N_4 membrane by stimulated decomposition and sputtering using a tightly focused electron beam about 1.6-2.0 nm (Gaussian width) in diameter in a JEOL 2010F transmission electron microscope (TEM) operating at 200keV. The pore geometry after sputtering has been visualized using reconstructed tilted TEM tomography as well as tilted HREM under various focus conditions. Although it is not unique, a simple model for the three-dimensional structure of the pore consists of two intersecting cones each with a cone angle of >15^{o}. After sputtering a pore through it, the membrane was mounted in a membrane transport bi-cell made from acrylic using silicone O-rings to seal the membrane to the acrylic (>5.0±0.2TΩ resistance). Each reservoir contains an *Ag/AgCl* electrode which is connected to an Axopatch 200B amplifier used in resistive feedback mode.

Prior work has indicated that the translocation velocity of *DNA* (not bound to a protein) through a *synthetic pore* may be large (~1bp/10 ns), making it difficult to resolve the transient associated with the translocation of short *DNA* strands across the membrane. A nanopore can be represented naively by an equivalent lumped element circuit consisting of a resistance associated with the pore, R_p, in parallel with the total membrane capacitance (including parasitics), C_m, and a series resistance, R_{el}, associated predominately with the electrolyte. Figure S1 shows the measured frequency performance obtained with 50 mV applied to a 2.5 nm diameter pore in a 12 nm thick nitride membrane spanning an area of 50 μmx 50 μm on an unintentionally-doped silicon chip sealed in a bi-cell with silicone washers about 1 mm in diameter. The frequency performance is measured using a sweep frequency generator along with a narrow-band lock-in amplifier to measure the ac current and noise as a function frequency. Generally, the current through the membrane consists of two components: one associated with the conductance through the pore, which predominates at low frequency; and another due to the displacement current associated with the membrane capacitance and associated parasitics. While both depend linearly on the applied voltage, the displacement current increases with frequency proportionally. Using this data, we can estimate the membrane capacitance from an oversimplified model that

effectively represents the nanopore as a lumped element circuit consisting of a capacitance associated with the membrane, C_m in parallel with the pore resistance R_p, all in series with a resistance R_{el} associated with the electrolyte. We find that C_m>400pF the 12 nm thick membrane in 100mM *KCl*.

The rms-current noise and the transient response time are both related to the membrane capacitance. The transient response is determined essentially by the product of C_m, which is >400 pF for a 12-15nm thick membrane, and R_{el}, which is ~10-100 kΩ for 10-100 mM *KCl,* so that $R_{el}C_m$ >4 - 40 μsec, corresponding to a bandwidth of Δf=1/(2π 400pFx10kΩ) < 40 kHz, while a response time <1 μsec is required to capture a current transient associated with 105 bp *DNA*. The large membrane capacitance also has a deleterious effect on the signal-to-noise ratio given by $\Delta I/I_{rms}$, where ΔI represents the change in the current due to the translocation of *DNA* across the membrane through the pore, and I_{rms} is the noise current. Preliminary MD simulations indicate that $\Delta I/I$<0.2 for a rupture, which translates to a ΔI~120pA for a 3nm diameter pore (in 100mM *KCl*).[29,30] Therefore, for signal-to-noise SNR>2, we need peak-to-peak noise <60pA or an rms value of I_{rms}~60pA/8=7.5pA. If dielectric noise predominates, then $I_{rms}^2 = 4kT\,DC_m\,\pi\,\Delta f^2$ where D is the dielectric loss constant (D~0.2 for our membranes). For a bandwidth Δf=< 40 kHz, we estimate that DC_m~1pF is required to detect a current signature, which is a factor x100 smaller than the membrane capacitance used here.

Protocol for Concentration of DNA and qPCR analysis.

We tested the permeability of *dsDNA* in solution with *Eco*RI through nanometer-diameter pores as a function of the applied voltage. We used two separate *dsDNA* strands:

1. a 105 bp *dsDNA* which is extracted from the pUC19 (NEB part # N3041S) vector with the sequence:

5'-TAAGT TGGGT AACGC CAGGG TTTTC CCAGT CACGA CGTTG TAAAA CGACG GCCAG T***GAAT TC****GAG CT*CGG TACCC GGGGA TCCTC TAGAG TCGAC CTGCA GGCAT-3' where the cognate site for *Eco*RI is highlighted in red; and

2. a 900 bp *DNA* strand, which is extracted from a pTWIN1 vector (NEB part # N6951S) using forward primer GAATGACATCATTGTACACA and reverse primer GCCAACTCAGCTTCCTTTCG to amplify a sequence that spans the *Eco*RI cognate (indicated in red below). Selected portions of the sequence are given below:

GAATGACATCATTGTACACAACGGAAGAGCCATGGGCGGCCGC***GAATTC***CTCG
AGGGCTCTTCCTGCATCACGGGAGATGCACTAGTTGCCCTACCCGAGGGCGA
GTCGGTACGCATCGCCGACATCGTGCCGGGTGCGCGGCCCAACAGTGACAAC
GCCATCGACCTGAAAGTCCTTGACCGGCATGGCAATCCCGTGCTCGCCGACC
GGCTGTTCCACTCCGGCGAGCATCCGGTGTACACGGTGCGTACGGTCGAAGG
TCTGCGTGTGACGGGCACCGCGAACCACCCGTTGTTGTGTTTGGTCGACGTCG
CCGGGGTGCCGACCCTGCTGTGGAAGCTGATCGACGAAATCAAGCCGGGCGA
TTACGCGGTGATTCAACGCAGCGCATTCAGCGTCGACTGTGCAGGTTTTGCCC
GCGGAAAACCCGAATTTGCGCCCACAACCTACACAGTCGGCGTCCCTGGACTG
GTGCGTTTCTTGGAAGCACACCACCGAGACCCGGACGCCCAAGCTATCGCCG
ACGAGCTGACCGACGGGCGGTTCTACTACGCGAAAGTCGCCAGTGTCACCGA
CGCCGGCGTGCAGCCGGTGTATAGCCTTCGTGTCGACACGGCAGACCACGCG
TTTATCACGAACGGGTTCGTCAGCCACGCTACTGGCCTCACCGGTCTGAACTC
AGGCCTCACGACAAATCCTGGTGTATCCGCTTGGCAGGTCAACACAGCTTATA
CTGCGGGAC*AATT*GGTCACATATAACGGCAAGACGTATAAATGTTTGCAGCCC
CACACCTCCTTGGCAGGATGGGAACCATCCAACGTTCCTGCCTTGTGGCAGCT
TCAATGACTGCAGGAAGGGGATCCGGCTGCTAACAAAGCCCGAAAGGAAGCT
GAGTTGGC

According to the specification of the Amicon filter a retention rate of >90% is typical for molecules >10kDa. The molecular weight of 900bp/105bp *dsDNA* we used in experiment is about 550/64kDa, which is not near the filter threshold. Nevertheless, we habitually check the filter retention anyway, especially since we are trying to give an accurate assessment of the threshold for permeation. The cumulative recovery we obtained following our current protocol (with three spin-downs) was on average 88.3% of the calibrated standards as derived from the intensity plots of 4 different *DNA* amounts: 40, 20, 10, and 4 ng, which is consistent with an expected >95% recovery rate per spin down. The specification on the filter is essentially the *same as this value* ~90%. Because we are interested in counting every molecule that translocates through the pore, we also calibrate the fluorescent intensity measured in the gel at very low dilution. We find 81% recovery even at the ~100 molecule level.

To establish unequivocally if *DNA* permeates through the pore, the *DNA* near the anode was analyzed using PCR and gel electrophoresis, and quantitative PCR (*qPCR*).

For agarose gel electrophoresis, 10 μl of the resulting extract was utilized and PCR carried out for 35 cycles. We routinely ran gels to establish crudely the voltage threshold, and also confirm proper amplification of the strand with positive and negative controls. Figure S2 shows a typical gel for the 2.0x3.6nm pore, which indicates a threshold exists for a membrane voltage between 1V and 2.5V. With 2.5V applied to the membrane, the intense fluorescent band clearly indicates 105bp DNA when compared with the 100bp reference ladder, and the positive controls run as a function of the concentration indicate that amount of *DNA* is between a 10^{-6} and 10^{-8} dilution or about about 10^{3}-10^{5} copies.

To ascertain the amount of *DNA* quantitatively, the anode solution was analyzed using *qPCR*, following to well-established protocols. qPCR is the gold standard for *DNA* detection; it has been shown to produce 1-10 copy resolution reliably.[11,18]SYBR Green I, a commonly used fluorescent *DNA* binding dye, was included in the qPCR reaction mix. SYBR Green I intercalates between the bases in *dsDNA* and the increase in fluorescence can be detected after each PCR cycle, which is proportional to the amount of *DNA*. With reference to established standard curves of known copy number and cycle thresholds, we can infer the *DNA* copy number from the anode side of the bi-cell. For qPCR, 2.5 μL of the resulting extract was used per well in conjunction with a SYBR Green qPCR reagent system (Applied Biosystems, Foster City, CA). *DNA* primers were then added to the corresponding wells and cycle thresholds determined by an Applied Biosystems 9700 qPCR machine.

Steered Molecular Dynamics (SMD) Simulations

The SMD force is applied to one end of the *DNA* fragment while the protein is restrained. In our simulations, the SMD force was applied along the *DNA* helix, which was aligned with the *z*-axis. The SMD force was computed as $F(t) = k_{SMD}[z_{SMD}(t) - z_{COM}(t)]$, where $z_{COM}(t)$ is the *z*-coordinate of the center of mass of the ten terminal bps (which are subject to the SMD force); $z_{SMD} = z_{COM}(0) + v_{SMD}t$, where v_{SMD} = 0.5 nm ns^{-1} is the SMD velocity; k_{SMD} = 50,000 kcal mol^{-1} nm^{-2}. Note that the SMD force varies with time. The protein's *α*-carbons were subject to the harmonic restraints (k_{restr} =10.0 kcal mol^{-1} nm^{-2}) that applied along the *z*-axis only. That is, the protein was able to freely

move in the direction perpendicular to the SMD force.

In addition to the standard SMD simulation, which below is referred to as the reference simulation, a series of "stopped-SMD simulations" were performed. A stopped-SMD simulation is simply a continuation of the constant-velocity SMD simulation in which the SMD velocity is set to zero. A stopped-SMD simulation produces an effect similar to a creep deformation: the period τ of high strain rate (v_{SMD} = 0.5 nm ns^{-1}) is followed by the period of low stain rate (v_{SMD} = 0 nm ns^{-1}). Hence, we characterize a particular stopped-SMD simulation by the time t (the duration of the reference simulation) the *Eco*RI–*DNA* complex was subject to a high strain rate.

The protein–*DNA* displacement was characterized as follows. First, we identified all pairs (ij) of non-hydrogen atoms such that atom i belongs to *DNA*, atom j belongs to the protein, and the average distance $\langle d_{ij} \rangle$ < 0.45 nm over the last 2 ns of the equilibration. Then the list of the atomic pairs was made symmetrical to comply with the symmetry of the *DNA*–protein complex. For example, if atom i from *DNA* strand A and atom j from protein monomer A satisfied the above conditions, we required that a pair of the same atoms on complementary chains, i.e. atom i from *DNA* strand B, and j from protein monomer B was also on the list. All pairs of atoms that did not have their symmetric counterparts in the initial selection were removed from the list. The final list included 100 pairs of atoms. Since some atoms were present in more than one pair, the final list contained 44 atoms of *DNA* (GC**GAATTC**, the cognate nucleotides are highlighted) and 68 atoms of *Eco*RI (Asn-85, Ser-86, Ser-87, Ile-88, Lys-89, Lys-113, Ala-138, Ala-139, Gly-140, Asn-141, Ala142, Arg-145, Lys-148, and Asn-149). The overall protein–DNA displacement was computed as $R = 1/n \sum_{(ij)}(d_{ij}-\langle d_{ij} \rangle)$, where the sum runs over all atom pairs from the list, n is the number of pairs, d_{ij} is the distance (nm) between atoms i and j, and $\langle d_{ij} \rangle$ is the equilibrium distance obtained by averaging the distance over the last 2 ns of equilibration. To compute the displacement R_i of a single nucleotide i relative to its equilibrium position in the protein–*DNA* complex, the average was taken over all atomic pairs that contained atoms of nucleotide i.

SMD simulations of EcoRI-DNA mutants

In the main text of the manuscript we state that the lack of the X-ray structures

depicting equilibrium conformations of the mutant variants of DNA-EcoRI does not allow the influence of the mutations on the rupture force to be directly determined from SMD simulations. Naively, one could expect that all single basepair mutants of EcoRI-DNA complex would have a similar three-dimensional structure. If that was that case, we could repeat our SMD simulations on all mutants by using as the initial condition the X-ray structure of the cognate complex incorporating the point mutations. Unfortunately, this approach does not work. The X-ray structures of the cognate and nonspecific BamHI-DNA assemblies (BamHI is functionally and structurally similar to *Eco*RI) clearly show that both *DNA* and the protein have different conformations. Hence, the change in affinity and, therefore, the rupture force is directly related to the change in the conformation of the *DNA*-protein complex. Moreover, previous MD study of *DNA-Eco*RI complex determined the direct non-bonded interactions between the DNA backbone and the protein as the dominant contribution to the binding energy [7]. The hydrogen bonds between the protein and *DNA* nucleotides were found to contribute only a minor fraction (<15%) of the total binding energy. Hence, one can expect some structural transformation to take place upon replacing one base pair in the cognate *DNA-Eco*RI complex with another. Unfortunately, the time scale of the MD method is too short to observe such structural transformations.

To test the above considerations, we mutated a single AT base pair in the cognate *DNA-Eco*RI complex at positions A5-B8 into CG (the nucleotide numbering is provided in the main text). In our nanopore experiments, the threshold bias for this mutation is roughly half of that for the cognate sequence. Prior to applying the SMD protocol, the system was equilibrated for 10 ns. During the equilibration the conformation of the *DNA* backbone and the adjacent protein residues did not change. The only structural change was partial breakup of the hydrogen bonds within the base pair A6-B7, which is adjacent to the mutated base. The conformation obtained at the end of the equilibration was subject to the constant-velocity (v=0.5nm/ns) SMD protocol. Two SMD simulations were performed, applying the force to opposite ends of the DNA fragment. The plot of the SMD force versus time (Figure S3) revealed no statistically significant drop in the rupture force. Similar simulations carried out starting from the X-ray structures of the cognate and nonspecific *DNA-Bam*HI systems showed a threefold decrease of the

rupture force. Hence, the luck of the X-ray structure for the mutant variants of *DNA-Eco*RI does not allow the influence of the mutations on the rupture force to be determined quantitatively in an MD simulation.

Detailed Analysis of Stopped-SMD Simulations

Figures S4(b,c) show that, in the reference SMD simulation, nucleotides B9 and A9 deviate from their original positions by ~0.25 nm early in the trajectory (at $t \approx 2$ and 3 ns, respectively). The distance R_{cutoff} = 0.25 nm is comparable to the size of a water molecule, and hence can be used as an approximate criterion of rupture. The average displacement of A9 and B9 remains close to R_{cutoff} at all times after the initial breakup. Nucleotide B2 deflects beyond R_{cutoff} briefly at t = 21 and 35 ns but does not break away irreversibly.

In the τ = 6 ns simulation—see Figures S4(e, f)—the parameter R for nucleotide B2 reaches 0.25 nm at t = 12 ns and continues to increase. The rupture of B2 is followed by B3 reaching $R \approx 0.25$ nm at 14 ns and stabilizing at this level. Other nucleotides remain in the vicinity of their equilibrium positions. It can be concluded that nucleotides 9, 2, and 3, from weak to strong in that order, bind most weakly to the protein. In that simulation, A2 and A3 do not break away because the *DNA* fragment subject to the SMD force is on the other side of the protein. Nucleotide A6 may break away, albeit reversibly, in the τ = 6 ns simulation at $t \approx 28$ ns. The increase of R for B3 from 0 to 0.25 nm correlates with the decrease of the SMD force between 6–12 ns. That drop of the force can hardly be attributed to any other nucleotide alone, although all of them may contribute so some extent.

After the weakest-bond nucleotides have been identified from the low-strain simulations, analysis of the simulations at higher values of τ reveal the relative strength of other interactions in the *DNA-Eco*RI complex. In the τ = 6.9 ns simulation (Figures S4(g, h)), nucleotides B4 and B5 break away at t = 15 ns, A4, A3, and A8 at 17 ns, A7 at 18 ns, and B6 at 19 ns. Over the same period of time, ~8–20 ns, the force drops five-fold (see Figure S4(a)). Since nucleotides B3 and A6 are relatively weakly bound to the protein, nucleotides 4, 5, 8, and 7, from weak to strong in that order, are responsible for the integrity of the complex at low strain (τ= 6 ns) but break away at a slightly higher

strain (τ=6.9 ns). The timeline of rupture at τ =7.5 ns in Figures S5(b, c) is similar to the τ = 6.9 ns case, with minor differences in the order of rupture (B6 breaks away between B4 and B5). Additionally, A2 breaks away at *t* = 17 ns and A5 at *t* = 23 ns. In the τ=8.4 ns simulation (Figures S5(e, f)), the complex continues to withstand a pulling force of about 200 pN with only one nucleotide, B8, remaining in its equilibrium position. The bonds to nucleotides B7 and A5 stay intact until *t* ≈ 29 and 26 ns, respectively, but they yield thereafter. As illustrated by Figures S5(g, h), the complex dissociates altogether in the τ = 10.5 ns simulation.

The rupture "schedule" of all nucleotides is summarized in Figure 6 (see main text of the paper), where nucleotides are listed approximately in the order they break away. This order is not exactly the same in all simulations; however, it is clear that the weakest bonds may be probed and revealed by the lowest strains. The strain is roughly proportional to the run time *t* of the reference simulation or to the start time τ of a stopped-SMD simulation. Therefore, the following exclusion procedure was used to list the bonds from weakest to strongest. First, we list nucleotides B9 and A9 that break up at *t* = 2 and 3 ns of the reference simulation, respectively. Then we consider the stopped-SMD simulation with the smallest τ = 5 ns and list the nucleotide B2, which breaks away at *t* = 21 ns. Then we consider the simulation with the next-lowest strain, τ = 6 ns, and include the nucleotides B3 and A6 in the list, and so on. Note that the ranking of the nucleotides already on the list is not modified when the higher-strain (larger τ) stopped-SMD simulations are considered. In this sense, the ranking of the nucleotides' bonds from weak to strong becomes unique; corrections, if any, might be revealed by additional stopped-SMD simulations with smaller increments of stopping time τ.

The above procedure has a straightforward physical sense. In experiment, the force applied to *DNA* may increase orders of magnitude slower than it does in a MD simulation. Therefore, each nucleotide that is weak enough to rupture at a low strain will have enough time to break up. Thus, weaker-bound nucleotides will be excluded from further specific protein–DNA interactions early in the rupture process, and only stronger-bound nucleotides will survive to face a larger strain. Slowly increasing strain conditions are better approximated by stopped-SMD simulations, in which the strain is

kept nearly constant for long periods of time, than by the reference SMD simulation where the strain increases with a constant rate.

To qualitatively rank the nucleotides and the base pairs they form in respect with the stability of the *DNA*-*Eco*RI complex, and thus predict the effect of mutation in those base pairs on the free energy of the dissociation of the complex, the following considerations should be taken into account. The nucleotide B8 is the last one to hold on upon a large deformation (τ=8.4ns) and to break away at τ=10.5 ns. Its complementary nucleotide A5 is the last one to break away in DNA chain A. Their symmetrical counterparts, nucleotides A8 and B5, break away only after a considerable exposure (> 10 ns) to a moderate strain (τ= 6.9ns). The decrease in the force may be correlated with the deflection of nucleotides B5 and A5 at τ=8.4ns (see Figures S5(e, f). Therefore, a mutation in both base pairs A5–B8 and A8–B5 may have the largest effect on the ability of the complex to withstand a large deformation. If just one of the base pairs A5–B8 and A8–B5 is mutated, the rupture force and energy will depend on the direction in which the *DNA* is pulled. Most experiments, such as the nanopore force spectroscopy experiments, involve however, a large number of *Eco*RI–*DNA* complexes, and both pulling directions will be encountered with equal probability. The measured rupture threshold will therefore be close to that corresponding to the breakup pathway with the lowest potential barrier. Therefore, a mutation in either one of the above base pairs will have a smaller effect compared to a simultaneous mutation in both base pairs, yet the largest of all single-point mutations.

Apart from nucleotides 5 and 8, nucleotides 6 and 7 exhibit the next-strongest bonding to the protein. In the simulation with τ = 7.5 ns, nucleotide B7 does not break away at all, while nucleotides A7 and, to lesser extent, A6 and B6 are among the last ones to break away. Moreover, parameter *R* for A6, A7, and B6 increases in line with the decrease in the force, which suggests that the yield of these nucleotides is the reason for the drop in the force. Therefore, a mutation in both base pairs A6–B7 and A7–B6 will have the next largest effect on the dissociation energy among two-point mutations, and a mutation in one of these base pairs will have the second-largest effect of all possible single-point mutations.

By analogy, we find the base pairs A4–B9 and A9–B4 in the third place of the

qualitative ranking ladder, as both nucleotides A4 and B4 are the strongest of all remaining nucleotides. The increase in their displacement parameters R in the simulation with t = 6.9 ns correlates with the three-fold drop in the force between t ≈ 8–16 ns. Nucleotides A9 and B9 break easily but still may somewhat contribute to the specific interaction because they do not deviate too far from their equilibrium positions. Finally, in the end of the ranking ladder go base pairs A3–B10 (A10–B3) and A2–B11 (A11–B2), in that order. Only one nucleotide of each of those base pairs is close enough to the protein to contribute to the specific interaction essential for the sequence recognition by the enzyme. As mentioned above, a mutation in both symmetrical base pairs may be expected to have a somewhat larger effect than a single-point mutation in one these base pairs. The above qualitative considerations are summarized in the Table S1 below (see also the Table 1 in the main part of the paper for comparison to the experimental data).

Table S1. Predicted influence of *DNA* mutations (single- and double-nucleotide polymorphisms) on the free bulk energy of dissociation, Δ*G*, in descending order. Experimental bulk Δ*G* are given for comparison when available. The last line corresponds to the wild-type sequence CGC **GAATTC** GCG (the nucleotides are numbered 1–12 in that order, left to right).

mutation position	effect	Δ*G*, kcal mol^{-1}
5 and 8	strongest	No specific binding
5 or 8	very strong	-4.9
6 and 7	stronger	
6 or 7	strong	-6.2
4 and 9	moderate	
4 or 9	moderate	-8.6
3 and 10	weak	
3 or 10	weak	-13.2
2 and 11	very weak	
2 or 11	very weak	
1 and 12	negligible	
1 or 12	negligible	
no mutation	reference	-15.2

FIGURE CAPTIONS:

FIGURE S1. Frequency response of the current measured through a 2.5 nm diameter pore in a 12nm thick nitride membrane. The frequency response can be modeled naively using a single capacitor representing the membrane.

FIGURE S2. A gel array showing the threshold for 105bp EcoRI-DNA variant containing the cognate sequence permeating a 2.0x3.6nm pore.

FIGURE S3. SMD simulations of cognate and mutant EcoRI-DNA systems. The mutant structure was built based on the X-ray structure of the cognate complex by replacing a TA basepair with GC.

FIGURE S4. Stopped SMD simulations with τ = 5.0–6.9ns. **(a)** SMD force for the reference and stopped SMD simulations. **(b,c)** Displacement parameter *R* for nucleotides of the *DNA* chain A (b) and chain B (c) for the stopped SMD simulation with τ = 5 ns. The vertical line indicates the start of the constant-strain regime, the horizontal line represents the cutoff breakup distance R_{cutoff} = 2.5 Å. **(d)** The nucleotide numbering and coloring convention. **(e, f)** Same for τ = 6.0 ns. **(g, h)** Same for τ = 6.9 ns.

FIGURE S5. Stopped SMD simulations with τ =7.5–10.5 ns. **(a)** SMD force for the reference and stopped SMD simulations. **(b,c)**Displacement parameter *R* for nucleotides of the *DNA* chain A (b) and chain B (c) for the stopped SMD simulation with τ =7.5 ns. The vertical line indicates the start of the constant-strain regime, the horizontal line represents the cutoff breakup distance R_{cutoff} = 2.5 Å. **(d)** The nucleotide numbering and coloring convention. **(e, f)** Same for τ = 8.4 ns. **(g, h)** Same for τ=10.5 ns.

FIGURE S6. MD simulation of the effective force on dsDNA in nanopore. (a-c) Snapshots of the simulated systems. (d) The effective force on dsDNA versus time at a 1V bias. The effective force was computed using the method described in Ref. 39.

Figure S1

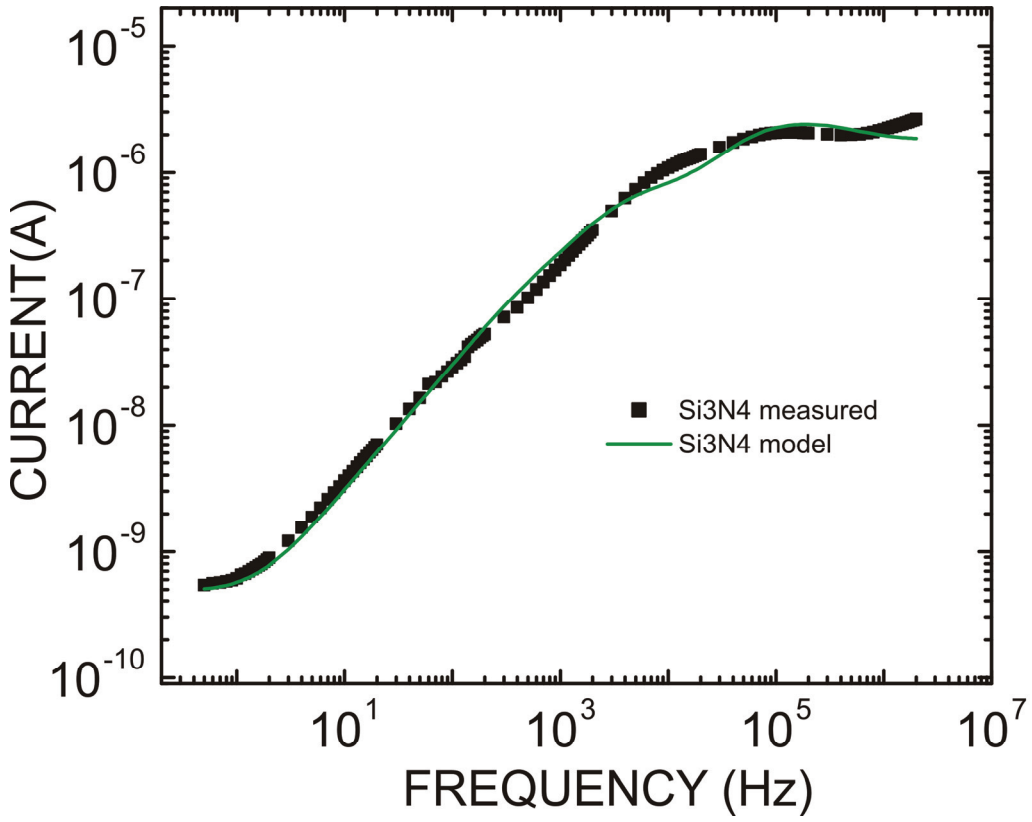
CURRENT(A)
10^-5
10^-6
10^-7
10^-8
10^-9
10^-10
10^1
10^3
10^5
10^7
FREQUENCY (Hz)
Si3N4 measured
Si3N4 model

Figure S2

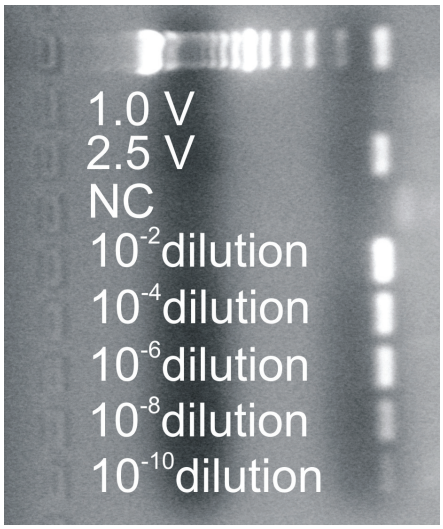
1.0 V
2.5 V
NC
10-2dilution
10-4dilution
10-6dilution
10-8dilution
10-10dilution

Figure S3

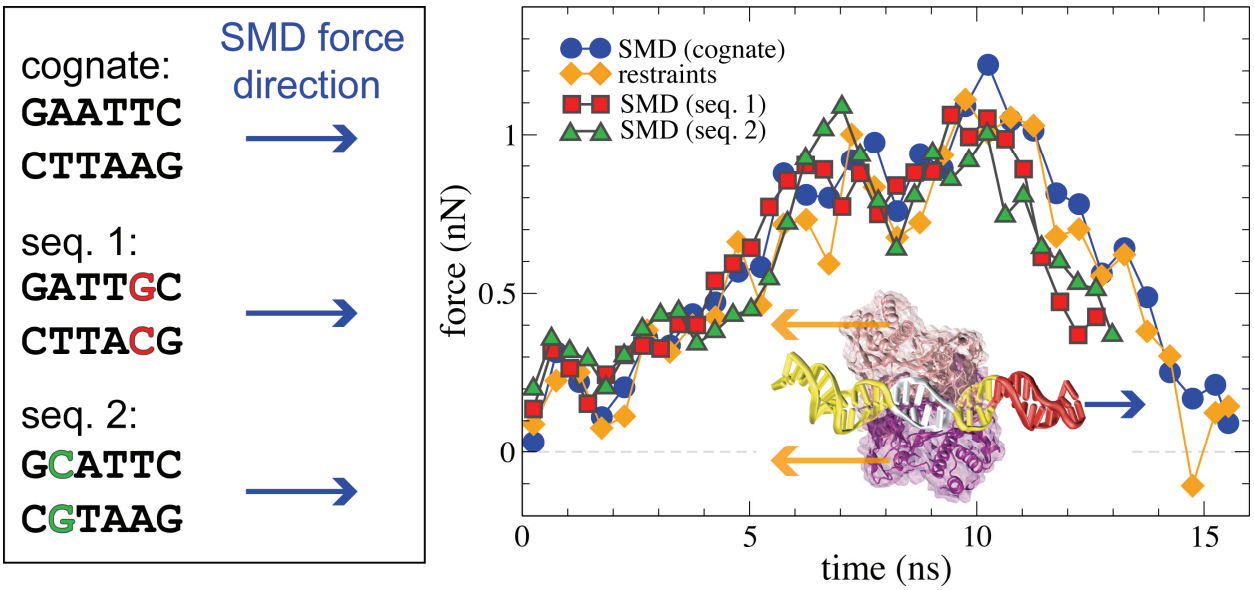
cognate:
GAATTC
CTTAAG
SMD force direction
seq. 1:
GATTGC
CTTACG
seq. 2:
GCATTC
CGTAAG
SMD (cognate)
restraints
SMD (seq. 1)
SMD (seq. 2)
force (nN)
time (ns)
0
0.5
1
0
5
10
15

Figure S4

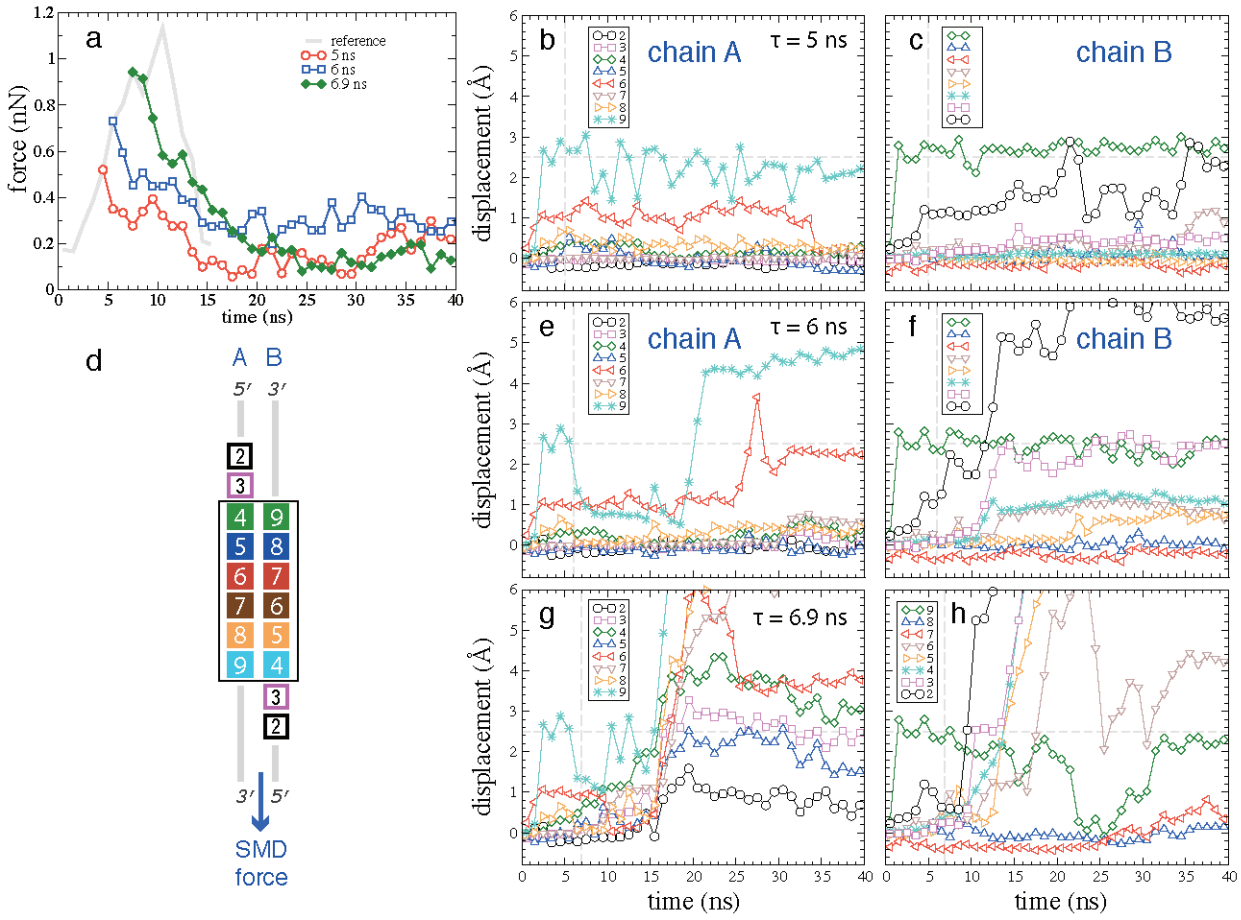
a
reference
5 ns
6 ns
6.9 ns
force (nN)
time (ns)
b
chain A
τ = 5 ns
c
chain B
e
chain A
τ = 6 ns
f
chain B
g
τ = 6.9 ns
h
displacement (Å)
time (ns)
d
A B
5′ 3′
SMD
force

Figure S5

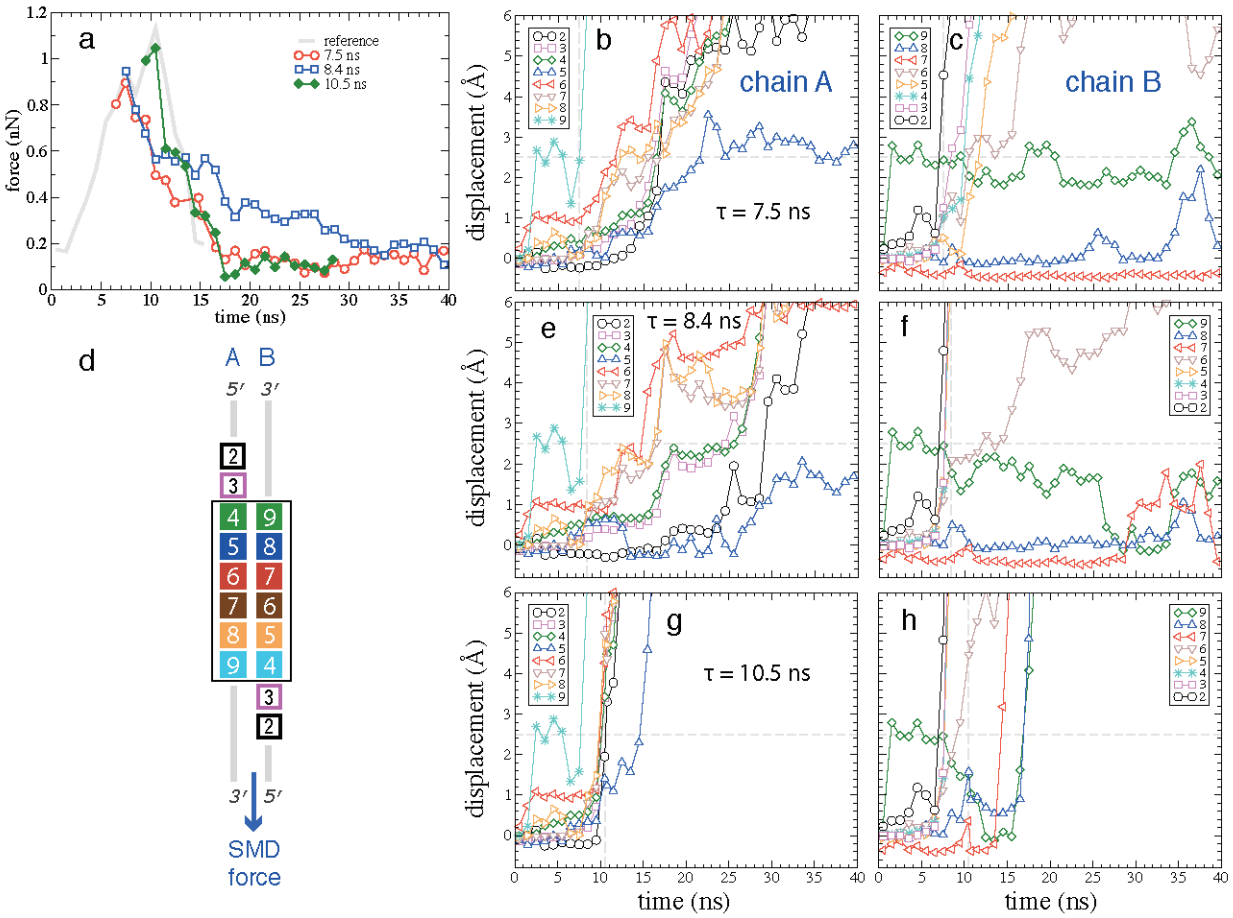
a
reference
7.5 ns
8.4 ns
10.5 ns
force (nN)
time (ns)
b
chain A
τ = 7.5 ns
c
chain B
d
A B
5′ 3′
SMD
force
e
τ = 8.4 ns
f
g
τ = 10.5 ns
h
displacement (Å)
time (ns)

Figure S6

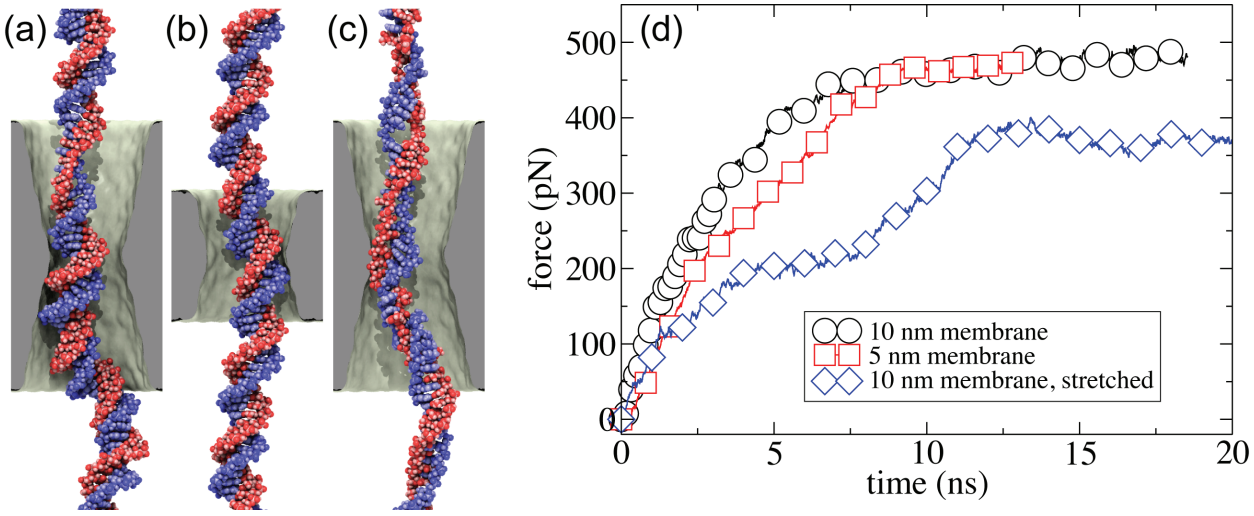
(a)
(b)
(c)
(d)
force (pN)
time (ns)
0
100
200
300
400
500
0
5
10
15
20
10 nm membrane
5 nm membrane
10 nm membrane, stretched